PROGRESS IN PHOTOVOLTAICS: RESEARCH AND APPLICATIONS
Prog. Photovolt: Res. Appl. (2012)
Published online in Wiley Online Library (wileyonlinelibrary.com). DOI: 10.1002/pip.2235

RESEARCH ARTICLE

Accurate explicit equations for the fill factor of real solar cells—Applications to thin-film solar cells

K. Taretto*, M. Soldera and M. Troviano

Dto. de Electrotecnia, Univ. Nacional del Comahue-CONICET, Buenos Aires 1400, 8300 Neuquén, Argentina

ABSTRACT

Even within the simplest real solar cell model, the exact value of the fill factor (FF) is only computable by numerical calculations. Here, we perform approximations to the power–voltage curve given by the one-diode model with series and shunt resistance losses, obtaining explicit expressions for the voltage and current at the maximum power point, and thus an explicit approach for the FF. Over a broad range of possible solar cell parameters, including cells where the impact of shunt losses on the fill factor is not negligible, the approximate equations yield relative errors typically around 1%. The equations are applied to explore the dependence of FF on alternative buffer material thickness of organic solar cells, and to investigate the incidence of shunt and series resistance losses on the FF of Cu(In,Ga)Se_2 solar cells under indoor illumination conditions. Copyright © 2012 John Wiley & Sons, Ltd.

KEYWORDS

fill factor equation; resistance losses; explicit one-diode model; organic solar cells; CIGS solar cells

***Correspondence**

Kurt Taretto, Dto. de Electrotecnia (FAIN), Universidad Nacional del Comahue-CONICET, Buenos Aires 1400, 8300 Neuquén, Argentina.
E-mail: kurt_taretto@yahoo.com

Received 3 August 2011; Revised 13 December 2011; Accepted 20 April 2012

1. INTRODUCTION

Solar cell development requires appropriate loss diagnoses based on measured output characteristics. A fundamental analysis consists in the fitting of current density–voltage *J(V)* curves using single or double-diode models to represent the equivalent electrical circuit of a solar cell [1–3]. In real solar cells, the electrical model also requires the inclusion of both series and parallel (or shunt) resistance losses [1,4]. Within the single-diode model of real solar cells, the implicit current density–voltage *J(V)* equation reads as follows:

$$J(V) = J_0\left[\exp\left(\frac{V - Jr_s}{AV_t}\right) - 1\right] + \frac{V - Jr_s}{r_p} - J_{ph} \quad (1)$$

Where J_0 is the reverse saturation current density, A the diode ideality factor, V_t the thermal voltage, J_{ph} the photocurrent density, r_s the specific series resistance and r_p the specific parallel (or shunt) resistance. The thermal voltage is given by $V_t = kT/q$, being k Boltzmann's constant, q the elementary charge, and T the device temperature. The knowledge of the parameters of Equation (1) allows quantifying the effect of the recombination losses represented by J_0 and A, and the resistance losses represented by r_s and r_p, on the fill factor (FF) and efficiency. Alternatively, Equation (1) helps to predict the potential to increase the efficiency when reducing each loss mechanism. At the maximum power point (MPP) of the *J(V)* curve, the corresponding current density J_{MPP} and voltage V_{MPP} yield the maximum power density $P_{MPP} = J_{MPP} \times V_{MPP}$, defining the FF as follows [5]:

$$FF = \frac{V_{MPP}J_{MPP}}{V_{OC}J_{SC}} \quad (2)$$

Where V_{OC} is the open-circuit voltage and J_{SC} the short circuit current density. With the incident power density P_{ph}, the power conversion efficiency η reads [5]:

$$\eta = \frac{V_{OC}|J_{SC}|FF}{P_{ph}} \quad (3)$$

Despite its simplicity, Equation (1) requires a numerical solution to obtain a *J(V)* curve. This reduces the power of analysis that would deliver a single equation of the efficiency as a function of the involved parameters. This restriction to numerical solutions motivated approximate models that led to a number of analytical expressions of the fill factor and efficiency of solar cells. In the review by Sánchez and

Araújo, several analytical models for the efficiency of solar cells are compared, aiming at concentrator solar cells [6]. Because the mentioned approaches neglect parallel resistance losses, such approximations are of great help mainly in the evaluation of high performance and concentrator solar cells, where the parallel resistance losses are normally negligible [1,7]. Obviously, r_p is not negligible in general: for example, in solar cells with much higher area than typical laboratory scale cells or photovoltaic modules, where r_p is much smaller, or in state-of-the-art organic solar cells [8–10], where parallel resistance losses cannot be neglected in order to explain the measured *J(V)* curves—even at a superficial level. Additionally, under low light intensity conditions (e.g., indoor illumination), parallel resistance losses play also a key role even in highly efficient Si [11] and Cu(In,Ga)Se_2 (CIGS) solar cells [12,13].

In this contribution, we deduce analytical expressions for J_{MPP} and V_{MPP} assuming series as well as parallel resistance losses in solar cells obeying Equation (1), enabling the analytical computation of the fill factor and, hence, of the efficiency. The final equations are expressed in terms of basic algebraic operations and elementary functions, such as exponential and logarithm functions. In Section 2, we present the theoretical lineout of the model, obtaining first the equations for fill factor and efficiency without resistance effects and then the equations considering resistance losses. The specific mathematical steps needed to arrive at the final equations are detailed in the Appendix. Section 3 gives brief application examples in the following: (a) the optimization of organic solar cells under sunlight operation; and (b) resistance effects in CIGS cells under low-irradiance conditions.

2. THEORY

Recently, Equation (1) has been reformulated into an explicit form by incorporating the Lambert W-function [14–16], being *J(V)* given by [16]:

$$J(V) = \frac{V - r_p(J_0 + J_{ph})}{r_p + r_s} + \frac{AV_t}{r_s} W\left[\frac{r_p r_s J_0}{AV_t(r_p + r_s)} \exp\left(\frac{r_p(r_s(J_0 + J_{ph}) + V)}{AV_t(r_p + r_s)}\right)\right] \quad (4)$$

Where W is the Lambert W-function, defined by the solution to the equation $z = W(z)\exp[W(z)]$. The inverse form of Equation (4), namely the *V(J)* curve, is given by [14]:

$$V(J) = r_p(J_0 + J_{ph}) + (r_s + r_p)J - AV_t W\left[\frac{r_p J_0}{AV_t} \exp\left(\frac{r_p(J + J_0 + J_{ph})}{AV_t}\right)\right] \quad (5)$$

Using these expressions, we obtain equations for the short-circuit current density $J_{SC} = J(0)$, and the open-circuit voltage $V_{OC} = V(0)$. Let us briefly show that both equations allow to express the current–voltage curve as a function of only three not directly measurable parameters, r_s, r_p, and A, eliminating the unknowns J_0 and J_{ph}. Indeed, when Equations (4) and (5) are equated to $J(0) = J_{SC}$ and $V(0) = V_{OC}$, respectively, we obtain a system of two equations, which yield the exact solutions

$$J_{ph} = \frac{\left[V_{OC} - (r_p + r_s)J_{SC}\left(e^{V_{OC}/AV_t} - 1\right)\right]e^{J_{SC}r_s/AV_t} - V_{OC}}{r_p\left(e^{(J_{SC}R_s + V_{OC})/AV_t} - 1\right)} \quad (6)$$

and

$$J_0 = \frac{(r_p + r_s)J_{SC} + V_{OC}}{r_p\left(e^{-J_{SC}R_s/AV_t} - e^{V_{OC}/AV_t}\right)} \quad (7)$$

In the following, we shall obtain expressions of V_{MPP} and J_{MPP} from the explicit equations for *J(V)* and *V(J)*, Equations (4) and (5), respectively. Although the Lambert W-function is well embedded in modern computational software, we are interested in finding expressions in terms of elementary functions, which are desirable in order to simplify the analysis by direct inspection of the equations, and also to enable their computation by non-specific software such as spreadsheets or curve-plotting software. For these purposes, we will make use of asymptotic approximations to W(z), which are given by [17–19]:

$$W(z) = \begin{cases} z & \text{for } z < e \\ \ln(z) - \ln[\ln(z)] & \text{for } z \geq e \end{cases} \quad (8)$$

Where we use the definition $e = \exp(1)$. Both approximations are asymptotically accurate in the specified ranges of the argument z.

2.1. Resistance-free solar cell

In order to obtain reference solutions and be introduced to the mechanics of using Equation (8), let us first solve the simplest case where no resistance losses occur, that is, setting $r_s = 0$ and letting $r_p \to \infty$ in Equation (1). We obtain the open circuit voltage

$$V_{OC} = AV_t \ln(1 + J_{ph}/J_0) \quad (9)$$

and the short-circuit current density $J_{SC} = -J_{ph}$. Because V_{OC} and J_{SC} are directly measurable quantities, one might use $J_{ph} = -J_{SC}$ and, from Equation (9), we obtain the saturation current density $J_0 = -J_{SC}[\exp(V_{OC}/AV_t) - 1]^{-1}$. This allows rewriting the resistance-free current–voltage equation as follows:

$$J(V) = J_{SC}\left[1 - \frac{\exp(V/AV_t) - 1}{\exp(V_{OC}/AV_t) - 1}\right] \quad (10)$$

When computing the power density $P = V \times J(V)$, we find the maximum delivered power point at the voltage V_{MPP} given by the following exact expression:

$$V_{MPP} = AV_t\{W[\exp(1 + V_{OC}/AV_t)] - 1\} \quad (11)$$

The exact current density J_{MPP} at the MPP is calculated replacing V_{MPP} in Equation (10). Equation (11) is readily simplified as it is sufficient that $V_{OC} > AV_t$ to turn the argument of the Lambert W-function greater than e. This allows to use the second asymptotic approximation (case $z \geq e$) of the Lambert W-function from Equation (8), yielding:

$$V_{MPP} \cong V_{OC} - AV_t \ln(1 + V_{OC}/AV_t) \quad (12)$$

This expression agrees with textbook equations [20] that use simplifications not relying on the exact expression of V_{MPP} involving W given by Equation (11). The error of V_{MPP} calculated with Equation (12) relative to the exact V_{MPP} delivered by Equation (11) is between 5 and 10% for a wide practical range of $V_{OC}/AV_t = 25$–10, respectively.

With V_{MPP} given by Equation (12), the approximate current–density at the MPP evaluated from Equation (10) yields

$$J_{MPP} \cong \frac{J_{SC}}{[1 - \exp(-V_{OC}/AV_t)](1 + AV_t/V_{OC})} \quad (13)$$

which correctly gives $J_{MPP} = J_{SC}$ in the limit $V_{OC}/AV_t \to \infty$. The fill factor is obtained evaluating Equation (2) using Equations (12) and (13), which, neglecting the exponential term in Equation (13), yields

$$FF \cong \frac{V_{OC}/AV_t - \ln(1 + V_{OC}/AV_t)}{1 + V_{OC}/AV_t} \quad (14)$$

which agrees with well known textbook formulas [20]. In the range $V_{OC}/AV_t = 10$–25, this equation gives FF with a relative error of 12–4%, respectively.

2.2. Real solar cell

In order to proceed to calculate the MPP, we make three simplifying assumptions, A1, A2, and A3, which read as follows:

A1. the photocurrent satisfies $J_{ph} >> J_0$,
A2. the parallel resistance is larger than the series resistance, $r_p > r_s$, and
A3. the open circuit voltage satisfies $3J_{ph}r_s < V_{OC} < \frac{2}{3}J_{ph}r_p$.

Note that A2 is valid for both non-optimized solar cells as well as optimized solar cells, which certainly will satisfy $r_p >> r_s$. The limits of A3 are shown in Figure 1, where we find the following $J(V)$ curves normalized to the resistance-free values of V_{OC} and $-J_{SC}$: reference with no resistance effects (curve 1), series resistance satisfying $3J_{ph}r_s = V_{OC}$ (curve 2), shunt resistance satisfying $\frac{2}{3}J_{ph}r_p = V_{OC}$ (curve 3), and series and parallel resistance where the conditions of both curves 2 and 3 are satisfied, that is, $3J_{ph}r_s = V_{OC} = \frac{2}{3}J_{ph}r_p$ (curve 4). All curves in Figure 1 were calculated with $A = 1.5$.

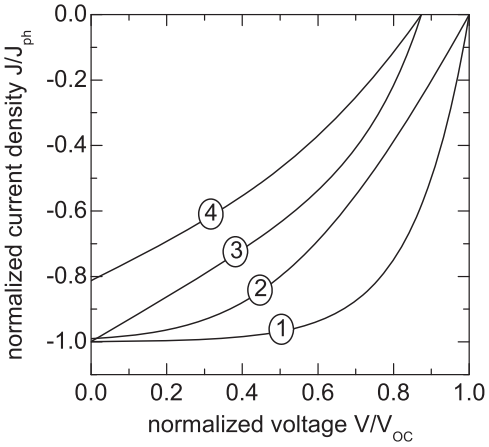

Figure 1. Sample normalized current–voltage curves of solar cells having the following: (1) no resistance effects, (2) a series resistance which satisfies $3J_{ph}r_s = V_{OC}$, (3) a shunt resistance satisfying $\frac{2}{3}J_{ph}r_p = V_{OC}$, and (4) a series and shunt resistance satisfying simultaneously the conditions of both (2) and (3). The approximate equations for the fill factor presented in the text cover curves (1)–(4) within a relative error between 1 and 5%.

In the following, assumptions A1–A3 are introduced in the solution process to obtain the MPP. Taking A1, Equation (4) becomes as follows:

$$J(V) = \frac{V - r_pJ_{ph}}{r_p + r_s} + \frac{AV_t}{r_s}W[f(V)] \quad (15)$$

Where the argument of the Lambert W-function $f(V)$ is given by:

$$f(V) = \frac{J_0r_s}{AV_t(1 + r_s/r_p)}\exp\left(\frac{J_{ph}r_s + V}{AV_t(1 + r_s/r_p)}\right) \quad (16)$$

Let us express $P(V) = V \times J(V)$ and differentiate with respect to V. In the derivation procedure, we must take into account the property $dW(z)/dz = z^{-1}W(z)/[1 + W(z)]$, obtaining:

$$\frac{dP(V)}{dV} = \frac{2V - J_{ph}r_p}{r_p + r_s} + \frac{AV_t}{r_s}W[f(V)] + \frac{V}{r_s}\frac{r_p}{r_p + r_s}\frac{W[f(V)]}{1 + W[f(V)]} \quad (17)$$

The voltage V_{MPP} corresponding to the MPP is the solution of $dP(V)/dV = 0$. In the Appendix, we show that around V_{MPP}, the "$2V$" in the first quotient of Equation (17) turns negligible, and also that assumption A2 leads to neglecting the second term of Equation (17). The resulting final approximate expression for V_{MPP} is given by:

$$V_{\mathrm{MPP}} \cong \left(1 + r_s/r_p\right)\left\{V_{OC} - AV_t \ln\left[\frac{V_{OC}}{AV_t} - \frac{2J_{ph}r_s}{AV_t\left(1 + r_s/r_p\right)}\right]\right\} - J_{ph}r_s \tag{18}$$

The current density J_{MPP} at the MPP results as follows:

$$J_{\mathrm{MPP}} \cong \frac{V_{\mathrm{MPP}} - J_{ph}r_p}{r_p + r_s} + \frac{J_0 r_p}{r_p + r_s}\exp\left(\frac{J_{ph}r_s + V_{MPP}}{\left(1 + r_s/r_p\right)AV_t}\right) \tag{19}$$

These equations allow to calculate the FF (Equation (2)) and conversion efficiency (Equation (3)) of real solar cells that satisfy assumptions A1–A3. We notice that both expressions are consistent with the "resistance-free" case, because with $r_s = 0$ and $r_p \to \infty$, Equation (18) correctly yields Equation (12) when $V_{\mathrm{OC}}/AV_t \gg 1$, and Equation (19) yields $J_{\mathrm{MPP}} = -J_{ph} + J_0\exp(V_{\mathrm{MPP}}/AV_t)$, which by replacing V_{MPP} from Equation (18) and letting $V_{\mathrm{OC}}/AV_t \gg 1$, yields $J_{\mathrm{MPP}} = -J_{ph} \cong J_{\mathrm{SC}}$.

Next, we show the error made when using the approximate expressions (18) and (19) to calculate the efficiency. The "exact" $\mathrm{FF_{ex}}$ is calculated using V_{MPP} from the numerical root of the derivative of the power density $\mathrm{d}(J \times V)/\mathrm{d}V = 0$, with the expression of $J(V)$ from Equation (4), which is then used to compute J_{MPP}. With the approximate $\mathrm{FF_{app}}$ obtained with Equations (18), (19) and (3), we calculate the relative error $e_r = 1 - \mathrm{FF_{app}}/\mathrm{FF_{ex}}$. In order to cover a broad range of possible situations, we consider combinations of high and low V_{OC} solar cells having high and low J_{SC}, across more than two orders of magnitude in r_s and r_p. Figure 2 shows a contour plot of the relative error e_r as a function of r_s and r_p for a cell having $V_{\mathrm{OC}} = 0.5\,\mathrm{V}$ and the short-circuit current densities indicated in each plot. The hatched horizontal/vertical areas belong to regions of the parameters where the r.h.s./l.h.s. of assumption A3 are not satisfied. Figure 3 shows corresponding contour plots of e_r in a solar cell with higher voltage $V_{\mathrm{OC}} = 0.75\,\mathrm{V}$, assuming the short circuit current densities indicated in each plot. Both Figures 2 and 3 were obtained considering an ideality $A = 1.5$, a thermal voltage $V_t = 25\,\mathrm{mV}$, and an incident power density $P_{ph} = 100\,\mathrm{mW/cm^2}$. Collectively, both Figures 2 and 3 show that with realistic combinations of low/high current and voltage solar cells and low/high series and shunt resistance effects, the present model yields values of the FF, and thus of the efficiency η, with a relative error typically around 1% and always below 5%.

3. APPLICATION EXAMPLES

Here, we show two brief examples where the present model is applied to practical solar cells. Both cases are aimed at highlighting the use of the model in cases where both series and parallel resistance losses have a non-negligible effect on the FF.

3.1. Optimization of electron contact layer thickness of organic solar cells

In organic photovoltaics, flexible organic solar panels are an attractive application that is currently approaching industrial status [21], despite the fact that research efforts towards optimization are still required. Organic polymer solar cells are typically prepared with indium-tin-oxide (ITO) as a highly convenient transparent electron contact material [22]. However, ITO seems not to be an optimum choice for flexible applications, because bending induces microscopic cracks in this layer—strongly reducing device efficiency. Therefore, investigation efforts are directed towards

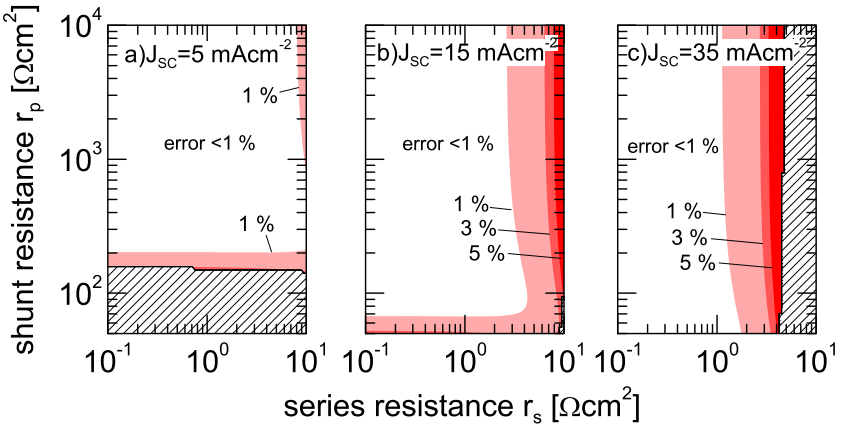

Figure 2. Contour curves of the relative error in the fill factor calculated from the approximate equations (18) and (19) and the "exact" fill factor obtained by root finding of Equation (17). The parameters assumed are an open circuit voltage $V_{\mathrm{OC}} = 0.5\,\mathrm{V}$, ideality $A = 1.5$, thermal voltage $V_t = 25\,\mathrm{mV}$, and the short-circuit current densities $J_{\mathrm{SC}} = 5$, 15 and $35\,\mathrm{mA\,cm^{-2}}$ corresponding to graphs (a), (b) and (c), respectively.

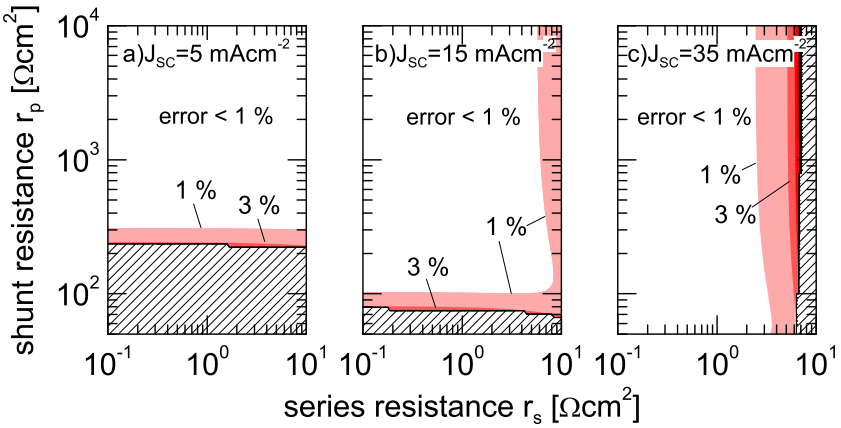

Figure 3. Calculation error in the fill factor calculated from the approximate equations (18) and (19) and the "exact" fill factor obtained by root finding of Equation (17). The parameters assumed are the open circuit voltage $V_{OC} = 0.75$ V, the ideality $A = 1.5$, the thermal voltage $V_t = 25$, and the short-circuit current densities $J_{SC} = 5$, 15 and 35 mA cm^{-2} corresponding to graphs (a), (b) and (c), respectively.

replacing ITO by alternative materials [23]. Recently, S. K. Hau and coworkers replaced the ITO layer in inverted-structure poly-3-hexylthiophene:[6,6]-phenyl-C61-butyric acid methyl ester (P3HT:PCBM) bulk heterojunction solar cells by a layer of the transparent polymer Poly(3,4-ethylene-dioxythiophene):poly(styrenesulfonate) (PEDOT:PSS) of various thickness [24]. Although they obtained no bending degradation, the lower conductivity of PEDOT:PSS compared with ITO required an optimization of the thickness of PEDOT:PSS, additionally taking into account the lower optical transmittance with increasing thickness [24]. Here, we analyze the data of Hau *et al.* using our model, mainly aiming at the dependence of the FF on resistance losses. Figure 4 shows the *J(V)* curves (data points) for different PEDOT:PSS thickness values, as reported in Reference [24], together with the corresponding fits (solid lines) we obtained using Equation (1). Table I gives the electrical output parameters $J_{SC} \cong -J_{ph}$, V_{OC} and FF of each cell, as well as the fit parameters r_s, r_p, A, and J_0, sorted according to the PEDOT:PSS thickness. The rightmost column shows the maximum fit error defined as the deviation between data points and fit curve. Evidently, the one-diode model is sufficient to accurately fit all of the *J(V)* curves, enabling to deepen the analysis within our model.

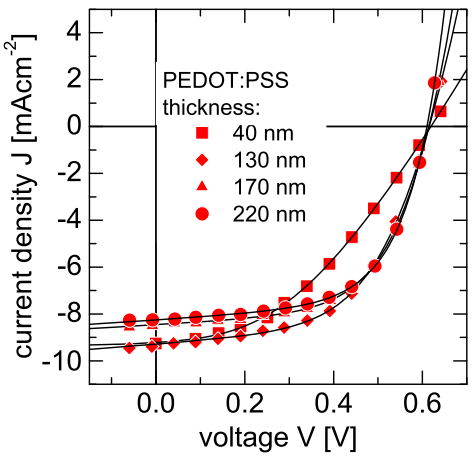

Figure 4. Illuminated current voltage curves of organic solar cells prepared using four different PEDOT:PSS thickness (symbols), fitted by the one-diode model (solid lines). The obtained solar cell output parameters and diode fit parameters are listed in Table I.

On the right axis of Figure 5, we read the reported PEDOT:PSS thickness (stars) as a function of the series resistance, clearly revealing the correlation of increasing resistance with decreasing PEDOT:PSS thickness. The left axis of Figure 5 shows the values of FF (red symbols) versus r_s, showing the decrease of FF with r_s. The decrease in FF is well reproduced by the solid line, which is calculated using Equations (18), (19) and (3) with the parameters $A = 3$, $V_t = 0.025$ mV, $r_p = 7.5 \times 10^2\ \Omega\,\text{cm}^2$,

Table I. Short-circuit current density J_{SC}, open circuit voltage V_{OC}, fill factor FF, series(parallel) resistance $r_s(r_p)$, diode ideality factor A, and saturation current density of organic solar cells reported in Reference [24] for various PEDOT:PSS layer thickness. The last column shows the maximum deviation error obtained from the fits shown in Figure 4.

PEDOT:PSS thickness (nm)	J_{SC} (A cm^{-2})	V_{OC} (mV)	FF [%]	r_s (Ω cm^2)	r_p (Ω cm^2)	A	J_0 (A cm^{-2})	Max. error (%)
40	92.6	619	40.4	2.6×10^1	6.7×10^2	3.07	3.9×10^{-6}	0.8
130	93.7	614	54.6	5.8×10^0	6.7×10^2	3.05	3.6×10^{-6}	0.6
170	84.8	613	58.4	2.8×10^0	8.9×10^2	3.02	3.0×10^{-6}	0.3
220	82.5	609	60.0	1.0×10^{-1}	7.8×10^2	3.02	3.0×10^{-6}	0.7

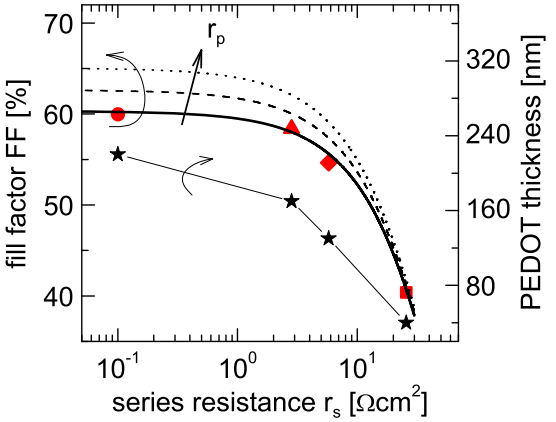

Figure 5. Fill factor (FF) (left axis) as a function of the series resistance r_s of the PEDOT:PSS layers, and correlation between PEDOT:PSS thickness with series resistance. The solid line over the FF data is given by the present model, explaining the decrease of FF with r_s, and the potential to increase FF by doubling the shunt resistance r_p (dashed line). The dotted line shows the limit to FF obtained for the limit $r_p \to \infty$, with the remaining parameters set equal to the solid line (see text for details).

$J_{ph} = 8.8\,\mathrm{mA\,cm^{-2}}$, $V_{OC} = 620\,\mathrm{mV}$. These values agree with the corresponding averages of the individual parameters extracted from the fits (Table I). The value of the saturation current density $J_0 = 2.08 \times 10^{-6}\,\mathrm{A\,cm^{-2}}$ was calculated with Equation (7) using the above parameters and $r_s = 10\,\Omega\,\mathrm{cm^2}$. This set of diode parameters satisfies assumptions A1–A3. As we can see in Figure 5, the model follows the observed behavior across two orders of magnitude of r_s. We notice that taking the shunt resistance r_p into account is critical to reproduce the FF data. Moreover, when calculating FF with a twofold parallel resistance, we obtain the dashed curve of Figure 5, and with $r_p \to \infty$, we get the ideal curve shown by the dotted curve. This allows to conclude that an optimization of the parallel resistance, for example, towards a twofold higher value, could increase the FF by 5% absolute (10% relative), provided the series resistance is kept below $10^0\,\Omega\,\mathrm{cm^2}$ using a PEDOT:PSS thickness above 170 nm.

3.2. Cu(In,Ga)Se_2 solar cells operated under indoor illumination

The high efficiency of 20.3% reached [25] by CIGS solar cells makes CIGS an attractive material not only for outdoor but also for indoor applications [13]. Indoor solar cells often work at very low irradiance conditions, resulting in higher incidence of the parallel resistance losses compared with standard outdoor conditions [11,13]. Here, we apply our model to explain the resistance losses under low intensity illumination of CIGS solar cells.

Three solar cells, two CIGS solar cells, labeled samples (a) and (b), and a Si solar cell as reference sample, were measured. The CIGS cells were prepared at the Institute for Photovoltaics (IPV) by the three stage process, which yields efficiencies up to 19% on a cell area of $0.5\,\mathrm{cm^2}$ [26]. The CIGS absorbers had Cu-poor composition, with an average Ga content Ga/(Ga + In) = 0.35. Details about the thickness of each layer and further deposition parameters are given in Reference [9]. The Si solar cell is a monocrystalline cell with diffused emitter and nitride anti-reflection coating. The cells were illuminated by a halogen-lamp combined with gray filters and variable distance between the source and the cells, obtaining three orders of magnitude in variation of the illumination intensity. For simplicity, we define a "1-sun" condition as the illumination intensity that yields a short current density of $36.4\,\mathrm{mA\,cm^{-2}}$ in the Si cell, which is the value measured at the IPE under standard $100\,\mathrm{mW\,cm^{-2}}$ illumination conditions [27]. A Keithley 2400 source-meter (Keithley Instruments, Inc., Solon, OH, USA) scanned the current–voltage curves at each illumination level, being the temperature of the cells controlled at 28 °C during the runs. Table II lists the efficiency obtained at 1-sun conditions, according to internal measurements performed at the IPE [27], and the diode parameters r_s, r_p, A, and J_0 of each cell under illuminated and dark (shown in parentheses) conditions, as explained later in the text.

Figure 6 shows the dependence of the open-circuit voltage V_{OC} (left axis) and the short-circuit current density J_{SC} (right axis) as a function of the illumination intensity given in suns, measured on the Si cell (diamonds), CIGS-a cell (circles), and CIGS-b cell (squares). We see that the V_{OC} versus the logarithmic illumination data practically follows a linear behavior, indicating that a single-diode model is sufficient to characterize the cells in the studied illumination range. Thus, we obtain the ideality factors given in Table II from the slope of linear fits to the V_{OC} versus illumination data (shown by the solid lines over the V_{OC} data). Collectively, the worse fit had a regression coefficient of $R = 0.997$, corresponding to the data of sample CIGS-a. We also obtained the diode parameters

Table II. One-sun efficiency η, series(parallel) resistance $r_s(r_p)$, diode ideality factor A, and saturation current density J_0 measured in three solar cells. The values of the diode parameters correspond to the illumination-dependent analysis (see text for details), whereas the values shown in parentheses belong to dark current–voltage fits.

Cell designation	η (1 sun)	r_s ($\Omega\,\mathrm{cm^2}$)	r_p ($\Omega\,\mathrm{cm^2}$)	A	J_0 ($\mathrm{A\,cm^{-2}}$)
Si	18.7	0.36(0.36)	∞	1.20(1.25)	(6.0×10^{-11})
CIGS-a	17.5	0.60(0.78)	$7.2(16) \times 10^3$	1.65(1.69)	(9.4×10^{-9})
CIGS-b	18.5	0.33(0.33)	$4.2(4.5) \times 10^3$	1.75(1.73)	(2.0×10^{-8})

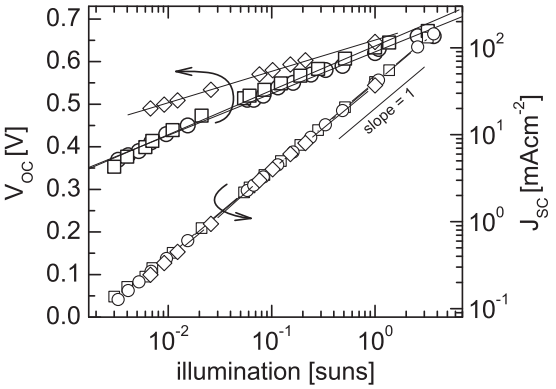

Figure 6. Open circuit voltage V_{OC} (left axis) and short circuit current density J_{SC} (right axis) as a function of illumination level for a Si solar cell (diamonds), CIGS-a cell (circles), and CIGS-b cell (squares). The observed linearity (straight lines across V_{OC} data) allows to assume a one-diode model to investigate the cells in the studied illumination range. See text for details.

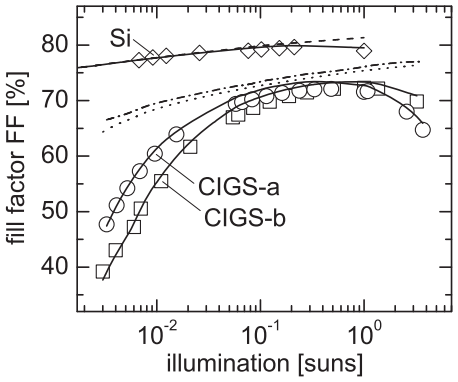

Figure 8. Fill factor (FF) as a function of illumination, measured on a Si solar cell (diamonds), and two CIGS cells (circles, squares). The solid lines are model fits assuming the diode parameters given in Table II, whereas the dashed, dash-dotted and dotted lines correspond to the case where no resistance effects are present. Comparing the resistance-free case to the data and model curves with resistance losses, the influence of shunt resistance at low illumination and series resistance at higher illumination levels is revealed.

by fitting the dark current–voltage curves shown in Figure 7 for cells CIGS-a (circles) and CIGS-b (squares), fitted by Equation (1) (solid lines). The corresponding fit parameters are found in Table II, given in parentheses. The diode parameters obtained by the illumination-dependent analysis are very close to the values obtained from the dark fits, further validating the analysis by the one-diode model.

Now, we proceed to explain the FF versus illumination dependence shown in Figure 8 for the measured Si cell (diamonds), CIGS-a cell (circles), and CIGS-b cell (squares). The solid lines in Figure 8 correspond to FF according to Equations (2), (18) and (19), using the parameters listed in Table II. The values of r_s and r_p are taken as parameters adjusting the FF curves, whereas the values of the saturation current density J_0 were calculated using V_{OC} and J_{SC} at each illumination value according to Equation (7), and are therefore not given in Table II. The good agreement between the model curves (solid lines) and the data confirm the validity of using the one-diode model in this dataset. In order to quantify the incidence of the resistance losses on FF, Figure 8 also shows the FF versus illumination curves obtained for the resistance-free case ($r_s = 0$ and $r_p \to \infty$) of each cell (dashed: Si cell, dash-dotted: CIGS-a, dotted: CIGS-b). Comparing the resistance-free curves with the solid lines and the data, we are able to conclude that the sharp decrease shown by the CIGS cells below 0.1 suns is explained by the effect of the shunt resistance alone, and that series resistance losses limit the FF around 1 sun conditions. We stress that the model is able to follow the shift between shunt to series-limited FF in a continuous fashion.

Figure 8 further indicates that the CIGS cells operated under indoor irradiation of, for example, 0.01 suns could improve the FF by up to 15% absolute by increasing r_p. As explained by Virtuani *et al*. in Reference [11], it is possible to explain the marked shunting behavior by the occurrence of shunting paths along grain boundaries in the CIGS absorber layer. A slightly smaller grain size would, in principle, interrupt the shunting paths, yielding a higher r_p, and therefore a reduced sensitivity of the cells to low intensity conditions—without sacrificing efficiency.

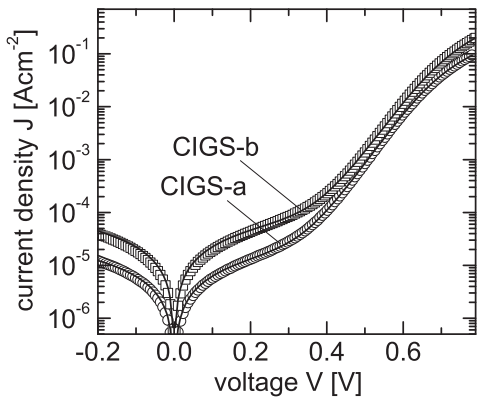

Figure 7. Dark current–voltage characteristics obtained for cells labeled CIGS-a (circles) and CIGS-b (squares), fitted by Equation (1) (solid lines), using the parameters listed in Table II in parenthesis.

4. CONCLUSIONS

We obtained closed-form expressions for the FF of real solar cells obeying a one-diode law with non-negligible series and parallel resistance losses. The obtained equations are expressed in terms of basic mathematical functions, providing a more accessible analysis capability than numerical solutions. This enables also to compute the

formulas using spreadsheets or non-specific computational software. We have shown that the FF is accurately computed by our equations, from very low efficiency solar cells where FF suffers from shunt resistance losses to high efficiency solar cells. For most practical cases, the equations yield a relative error in FF below 1% and up to 5% in cells highly dominated by either parallel or series resistance losses.

The use of the equations is exemplified in two practical cases: the optimization of the fill factor adjusting the thickness of the transparent electron contact layer and parallel resistance losses in organic bulk heterojunction solar cells, and the investigation of resistance effects in CIGS cells under low-irradiance conditions. Both examples show that the inclusion of both series and parallel resistance losses are mandatory to explain the experimentally observed behavior and to estimate the improvement potential associated to resistance losses.

ACKNOWLEDGEMENTS

The authors are grateful to J. Mattheis and J.-H. Werner from the Institut für Photovoltaik (http://www.ipv.uni-stuttgart.de/), who kindly provided the cells for the tests, and U. Rau and T. Kirchartz for continuous support. This work was supported by CONICET and Comahue National University (Argentina).

REFERENCES

1. Green MA. *Solar Cells*. University of New South Wales: Kensington, 1992; ch. 5.
2. Nelson J. *The Physics of Solar Cells*. Imperial College Press: London, 2003; 9–15.
3. Smestad GP. *Optoelectronics of Solar Cells*. SPIE Publications: Bellingham, 2002; 37–41.
4. Schroder DK. *Semiconductor Material and Device Characterization*. Wiley: Hoboken, 2006; 192–197.
5. Sze SM, Ng KK. *Physics of Semiconductor Devices* (3rd edn). Wiley: Hoboken, 2007; 724.
6. Sánchez E, Araújo GL. On the analytical determination of solar cell fill factor and efficiency. *Solar Cells* 1987; **20**: 1–11.
7. Algora C. *In Concentrator Photovoltaics*, Luque ALL, Andreev VM (eds). Springer: Berlin, 2010; 95.
8. Tumbleston JR, Ko DH, Samulski ET, Lopez R. Non-ideal parasitic resistance effects in bulk heterojunction organic solar cells. *Journal of Applied Physics* 2010; **108**: 084514-1–084514-8.
9. Potscavage WJ, Yoo S, Kippelen B. Origin of the open-circuit voltage in multilayer heterojunction organic solar cells. *Applied Physics Letters* 2008; **93**: 193308-1–193308-3.
10. Rand BP, Burk DP, Forrest SR. Offset energies at organic semiconductor heterojunctions and their influence on the open-circuit voltage of thin-film solar cells. *Physical Review B* 2007; **75**: 115327-1–115327-11.
11. Virtuani A, Lotter E, Powalla M. Performance of Cu(In,Ga)Se_2 solar cells under low irradiance. *Thin Solid Films* 2003; **431–432**: 443–447.
12. Reich NH, van Sark WG, Alsema EA, Lof RW, Schropp REI, Sinke WC, Turkenburg WC. Crystalline silicon cell performance at low light intensities. *Solar Energy Materials and Solar Cells* 2009; **93**: 1471–1481.
13. Virtuani A, Lotter E, Powalla M, Rau U, Werner JH, Acciarri M. Influence of Cu content on electronic transport and shunting behavior of Cu(In,Ga)Se_2 solar cells. *Journal of Applied Physics* 2006; **99**: 014906-1–014906-111.
14. Ortiz-Conde A, García Sánchez FJ, Muci J. Exact analytical solutions of the forward non-ideal diode equation with series and shunt parasitic resistances. *Solid State Electronics* 2000; **44**: 1861–1864.
15. Ortiz-Conde A, García Sánchez FJ, Muci J. New method to extract the model parameters of solar cells from the explicit analytic solutions of their illuminated *I–V* characteristics. *Solar Energy Materials and Solar Cells* 2006; **90**: 352–361.
16. Jain A, Kapoor A. Exact analytical solutions of the parameters of real solar cells using Lambert W-function. *Solar Energy Materials and Solar Cells* 2004; **81**: 269–277.
17. Barry DA, Culligan-Hensley PJ, Barry SJ. Real values of the W-function. *ACM Transactions on Mathematical Software* 1995; **21**: 161–171.
18. de Bruijn NG. *Asymptotic Methods in Analysis*. North-Holland: Amsterdam, 1958; 25–28.
19. Corless RM, Gonnet GH, Hare DEG, Jeffrey DJ, Knuth DE. On the Lambert W function. *Advances in Computational Mathematics* 1996; **5**: 329–359.
20. Würfel P. *Physics of Solar Cells: From Principles to New Concepts*. Wiley-VCH: Weinheim, 2005; 138.
21. Krebs FC, Jørgensen M, Norrman K, Hagemann O, Alstrup J, Nielsen TD, Fyenbo J, Larsen K, Kristensen J. A complete process for production of flexible large area polymer solar cells entirely using screen printing—first public demonstration. *Solar Energy Materials and Solar Cells* 2009; **93**: 422–441.
22. Guillén C, Herrero J. High performance electrodes for organic photovoltaics. In *Organic Photovoltaics*, Brabec C, Dyakonov V, Scherf U (eds). Wiley-VCH: Weinheim, 2008; 401–423.
23. Na S, Kim S, Jo J, Kim D. Efficient and flexible ITO—free organic solar cells using highly conductive polymer anodes. *Advanced Materials* 2008; **20**: 4061–4067.

24. Hau SK, Yip H-L, Zou J, Jen AK-Y. Indium tin oxide-free semi-transparent inverted polymer solar cells using conducting polymer as both bottom and top electrodes. *Organic Electronics* 2009; **10**: 1401–1407.
25. Jackson P, Hariskos D, Lotter E, Paetel S, Wuerz R, Menner R, Wischmann W, Powalla M. New world record efficiency for Cu(In,Ga)Se_2 thin-film solar cells beyond 20%. *Progress in Photovoltaics: Research and Applications* 2010; DOI: 10.1002/pip.1078
26. Jackson P, Würz R, Rau U, Mattheis J, Kurth M, Schlötzer T, Bilger G, Werner J-H. High quality baseline for high efficiency $CuIn_{1-x}Ga_xSe_2$ solar cells. *Progress in Photovoltaics: Research and Applications* 2007; **15**: 507–519.
27. Mattheiss J. formerly Institut für Physikalische Elektronik (http://www.ipv.uni-stuttgart.de/), 2005: personal communication.

APPENDIX

We start by showing that around V_{MPP}, $f(V_{MPP}) < e$ if assumption A3 is valid, that is $3J_{ph}r_s < V_{OC} < \frac{2}{3}J_{ph}r_p$. This condition, according to Equation (8), allows to express $W[f(V)] = f(V)$, as required. Evaluated at V_{MPP}, Equation (16) yields:

$$f(V_{MPP}) = \frac{J_0 r_s}{AV_t(1 + r_s/r_p)} \exp\left(\frac{J_{ph}r_s + V_{MPP}}{AV_t(1 + r_s/r_p)}\right) \quad (A.1)$$

Next, we show the conditions under which $f(V_{MPP}) < e$, considering the "resistance free" V_{MPP} from Equation (12) as a worst case approach that gives the highest $f(V_{MPP})$. This procedure yields conditions in terms of V_{OC} that cover $f(V_{MPP}) < e$ in excess, that is, conservatively. In Equation (A.1), we replace $J_0 = J_{ph}\exp(-V_{OC}/AV_t)$ and also V_{MPP} by Equation (12), obtaining:

$$f(V_{MPP}) = \frac{r_s J_{ph}\exp(-V_{OC}/AV_t)}{AV_t(1 + r_s/r_p)} \exp\left(\frac{J_{ph}r_s + V_{OC} - AV_t\ln(1 + V_{OC}/AV_t)}{AV_t(1 + r_s/r_p)}\right) \quad (A.2)$$

neglecting r_s/r_p for simplicity and simplifying the exponents yields:

$$f(V_{MPP}) = \frac{J_{ph}r_s}{V_{OC} + AV_t} \exp\left(\frac{J_{ph}r_s}{AV_t}\right) \quad (A.3)$$

With this expression, we find that the condition $f(V_{MPP}) < e$ is fulfilled when

$$V_{OC} > J_{ph}r_s \exp\left(\frac{J_{ph}r_s}{AV_t} - 1\right) - AV_t \quad (A.4)$$

Because even in low efficiency, non-optimized solar cells, the relations $V_{OC} > J_{ph}r_s$ and $V_{OC} > AV_t$ are satisfied simultaneously, the condition $J_{ph}r_s >> AV_t$ is excluded. This observation means that the exponent in Equation (A.4) is not much larger than one. Additionally, if we bear in mind that V_{OC} in Equation (A.4) stems from the V_{MPP} without resistance effects, we realize that cells with high $J_{ph}r_s$ actually have a considerably smaller V_{MPP}, satisfying $f(V_{MPP}) < e$ with smaller values of V_{OC} than the required by Equation (A.4). Thus, we adopt $V_{OC} > 3J_{ph}r_s$ as practical and compact variant to Equation (A.4), establishing the l.h.s. of assumption A3 given in the main text. In the limit $V_{OC} = 3J_{ph}r_s$, a relative error of 5% is introduced by Equations (18) and (19) in the fill factor, as shown in Figures 2(c) and 3(c).

Next, we discuss the additional simplifications to Equation (17) that lead to Equation (18). According to the condition shown above leading to $W[f(V)] = f(V)$, we rewrite Equation (17) at the maximum power point as follows:

$$\frac{dP(V_{MPP})}{dV} = \frac{2V_{MPP} - J_{ph}r_p}{r_p + r_s} + \frac{AV_t}{r_s} f(V_{MPP}) + \frac{V_{MPP}}{r_s}\frac{r_p}{r_p + r_s}\frac{f(V_{MPP})}{1 + f(V_{MPP})} = 0 \quad (A.5)$$

Because we are under the condition $f(V_{MPP}) < e$, we notice that the quotient containing $f(V_{MPP})$ in the last term of this expression tends asymptotically to $f(V_{MPP})$ with decreasing V_{MPP}. Thus, the second term containing AV_t is neglected, because $AV_t < V_{MPP}$. We may now rewrite the simplified Equation (A.5) in the more convenient form:

$$\frac{2V_{MPP}}{r_p} - J_{ph} + \frac{V_{MPP}}{r_s}\frac{f(V_{MPP})}{1 + f(V_{MPP})} = 0 \quad (A.6)$$

In this expression, we neglect the first term, but with the condition that $(2V_{MPP}/r_p) < J_{ph}$, that is avoiding the sign reversal of the root (the last term is always positive). Similarly to the analysis earlier, a more practical means of establishing this condition comes into light when evaluating V_{MPP} using Equation (12), leading to the condition $V_{OC} < \frac{2}{3}J_{ph}r_p$, that is the r.h.s. of assumption A3 in the main text. After neglecting the term $2V_{MPP}$ in Equation (A.6) and replacing $f(V_{MPP})$ by Equation (A.1), the approximate expression of the voltage at the maximum power point is given by:

$$V_{\mathrm{MPP}} \cong J_{ph} r_s + A V_t \left(1 + r_s/r_p\right) W\left[\frac{J_{ph}}{J_0} \exp\left(\frac{-2 J_{ph} r_s}{A V_t \left(1 + r_s/r_p\right)}\right)\right] \tag{A.7}$$

In this expression, it is possible show that with assumption A3, the argument in the Lambert W-function is larger than e, in which case, we resort to the asymptotic approximation $\mathrm{W}(z) \cong \ln(z) - \ln[\ln(z)]$ from Equation (8), and assuming $J_{ph}/J_0 = \exp(V_{\mathrm{OC}}/AV_t)$, we immediately obtain V_{MPP} given by Equation (18) from the main text. It can be shown that with $V_{\mathrm{OC}} < \frac{2}{3} J_{ph} r_p$, the error in assuming this approximation of J_{ph}/J_0 is below 12% relative. Finally, we notice that it is possible to show analytically the consistency of $f(V_{\mathrm{MPP}}) < e$ when V_{MPP} is evaluated from Equation (18).

DOI: 10.1002/pip